Janus Hybramers: Self-Adapting Amphiphilic Hyperbranched Polymers

ARTICLE *in* MACROMOLECULES · FEBRUARY 2012

Impact Factor: 5.8 · DOI: 10.1021/ma2022277

Macromolecules

Article

pubs.acs.org/Macromolecules

Janus Hybramers: Self-Adapting Amphiphilic Hyperbranched Polymers

Ashok Zachariah Samuel and S. Ramakrishnan*

Department of Inorganic and Physical Chemistry, Indian Institute of Science, Bangalore 560012, India

Supporting Information

ABSTRACT: Janus structures have attracted a great deal of interest because of their fascinating properties and potential for applications. In this study, we demonstrate that hyperbranched polymers, bearing randomly placed docosyl (C22 alkyl segment) and PEG segments on their periphery, can readily reconfigure so as to segregate the alkyl and PEG segments, thereby generating Janus-type structures that we have termed *Janus hybramers*. DSC studies clearly reveal an endothermic transition that corresponds to the melting of the docosyl domains, while Langmuir isotherms demonstrate that these polymers form stable monolayers that appear to undergo a slight densification beyond a critical surface pressure; this suggested possible crystallization of the docosyl segments at the air−water interface. AFM studies of the transferred monolayers reveal various interesting aggregate morphologies at different surface pressures suggestive of island formation at the air−water interface; at the same time they also provided an estimate of the monolayer thickness. These Janus HBPs also form vesicles as evident from TEM and AFM studies; the AFM height of the deposited vesicles, as expected, was roughly 4 times that of the monolayer. SAXS studies revealed the formation of lamellar structures; the interlamellar spacing was largest when the relative mole fractions of docosyl and PEG segments were similar, but the spacing decreased when the mole fraction of either of these peripheral segments is substantially smaller; this suggested the possible presence of interdigitation within the domains of the minor component.

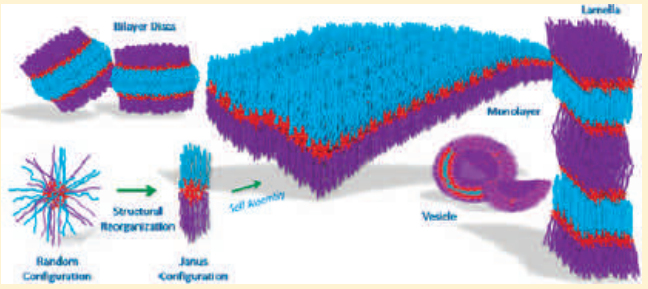

INTRODUCTION

Self-assembly of molecular systems has received a great deal of attention not only because of its fundamental importance in understanding cellular evolution[1] but also because understanding biological systems helps design nanoscale "smart materials" that mimic biological functions.[2] From this perspective, well-defined molecular architectures based on simple amphiphiles,[3] block copolymers,[4] dendrimers,[5] linear−dendritic blocks, hyperbranched polymers,[6] and other dendronized structures[7] have been extensively studied. Janus architectures have recently drawn a lot of attention because of the fascinating range of structural variability.[8] Müller and co-workers have pioneered the efforts to prepare polymeric Janus nanoparticles by exploiting the rich range of phase-separated morphologies formed by ABC type triblock copolymers; they have used selective cross-linking within the central B-block to generate a variety of Janus nanoparticles, ranging from spheres, cylinders to disks.[9−14] While all of these approaches generate Janus nanoparticles using an aggregate of polymer chains, the synthesis of readily tunable Janus molecular analogues has remained a difficult synthetic challenge. Janus dendrimers, which carry hydrophilic and hydrophobic units on either sides of their molecular periphery, is one exception that has been known for over a decade now.[15−19] However, there are only limited reports that describe their self-assembly properties. Recently, Percec and co-workers have carried out exhaustive studies to examine the self-assembly of a variety of lower generation Janus dendrimeric structures.[8] While dendrimers possess elegant structural symmetry, there is growing evidence that several functional properties may not require such rigorous structural perfection. Yan and co-workers, for instance, have demonstrated the self-assembly of polydisperse core−shell type hyperbranched polymers (HBPs) into tubes, micelles, and vesicles;[20] this proves undeniably that the monodisperse and structurally perfect molecular architectures are not essential criteria for generating self-assembled nanostructures. Several examples of core−shell domain separation in suitably designed hyperbranched polymers also provide evidence for conformational adaptability of the flexible hyperbranched backbone and their tolerance to high defect levels.[21−24] Additionally, studies by Tsukruk and co-workers have clearly shown that amphiphilic core−shell type HBPs reconfigure to jellyfish-like structures.[25,26] An interesting example of solvent-dependent self-adapting dendrimers was described by Aathimanikandan et al., wherein they showed that lower generation dendrimers carrying hydrophobic and hydrophilic segments on each repeat unit can conformationally readapt to enable solublity in both nonpolar and polar solvents.[27] In this context, it would be

Received: October 4, 2011
Revised: February 10, 2012
Published: February 27, 2012

   dx.doi.org/10.1021/ma2022277 | *Macromolecules* 2012, 45, 2348−2358

interesting to pose the question: *Can hyperbranched polymers, wherein peripheral end groups are randomly functionalized by hydrophobic and hydrophilic segments, conformationally readapt to form Janus structures, as depicted below?* Very recently, Chute et al. have suggested, based on a computational study, that reorganization to Janus-type structures is unlikely in the extreme case of dendrimers that bear hydrophobic and hydrophilic segments on each of their terminal units.[28] In an effort to address this question experimentally, we describe studies on hyperbranched (HB) polyesters, whose peripheral propargyl groups have been randomly clicked with both hydrophobic and hydrophilic segments. The parent polymer was synthesized using our recently developed single-step synthesis for the generation of peripherally clickable hyperbranched polyesters.[29] On the basis of their behavior in solution, at the air−water interface, small-angle X-ray scattering (SAXS), and differential scanning calorimetric (DSC) studies, we provide concrete evidence to demonstrate that hyperbranched polymers carrying randomly clicked hydrophobic and hydrophilic segments do indeed readapt to exhibit Janus-type behavior.

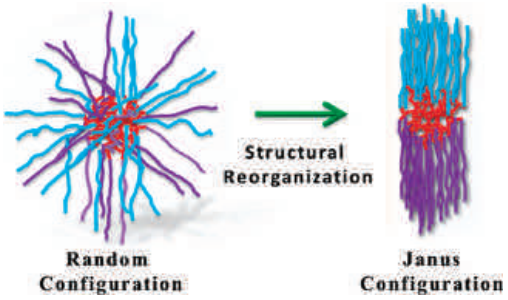

RESULTS AND DISCUSSION

The parent peripherally clickable hyperbranched polyester was prepared from monomer **A** via a melt transesterification process, as depicted in Scheme 1; the monomer was prepared readily from 5-hydroxyisophthalic acid.[29] The polymer exhibited a very broad molecular weight distribution—M_w = 84 000 and M_n 5600—which is often seen in the case of hyperbranched polymers prepared via the self-condensation of AB_2 type monomers. The degree of branching (DB) of the polyester could not be readily estimated; however, based on an earlier report by Feast et al.,[30] on a similar HB polyester we believe the value would be around 60%. This single-step process provides an attractive route to access useful molecular scaffolds on to which a variety of units could be clicked using the versatile copper-catalyzed quantitative azide−yne reaction.[31] In order to prepare amphiphilic systems, the clickable polyester scaffold was treated with two different azides, namely docosyl azide (a linear C-22 alkyl azide) and PEG-350 monomethyl ether azide. Polymers containing three different compositions of these hydrophobic and hydrophilic segments were thus prepared; these have been labeled as DOCOPEG-*xy*, where *x* and *y* represent the mole percentage of docosyl azide and PEG azide, respectively, used during the click reaction. In principle, two approaches could be taken to prepare these amphiphilic hyperbanched structures: one where the docosyl azide and the PEG azide are clicked sequentially and the second where both of the azides are taken in the required mole ratio and clicked simultaneously. We chose the latter approach as we expected this to produce a more randomly clicked structure (with a homogeneous distribution of PEG and docosyl groups on the periphery).

The proton NMR spectra of the parent clickable polyester (HBP-PE) carrying propargyl ester groups at the periphery, along with one that was clicked with docosyl azide and PEG azide in the mole ratio 70:30 (DOCOPEG-7030), are shown in Figure 1; the peaks are assigned as shown in the figure. It is evident that the click reaction has gone to completion, as no peaks due to residual propargyl groups (at ∼2.55 and 4.95 ppm) are seen in the spectrum of the clicked polymer. The peaks due to the terminal methyl protons of the docosyl and PEG units, at

Scheme 1. Synthesis of Clickable Hyperbranched Polyesters and Their Derivatization To Generate Amphiphilic DOCOPEG-*xy* Systems

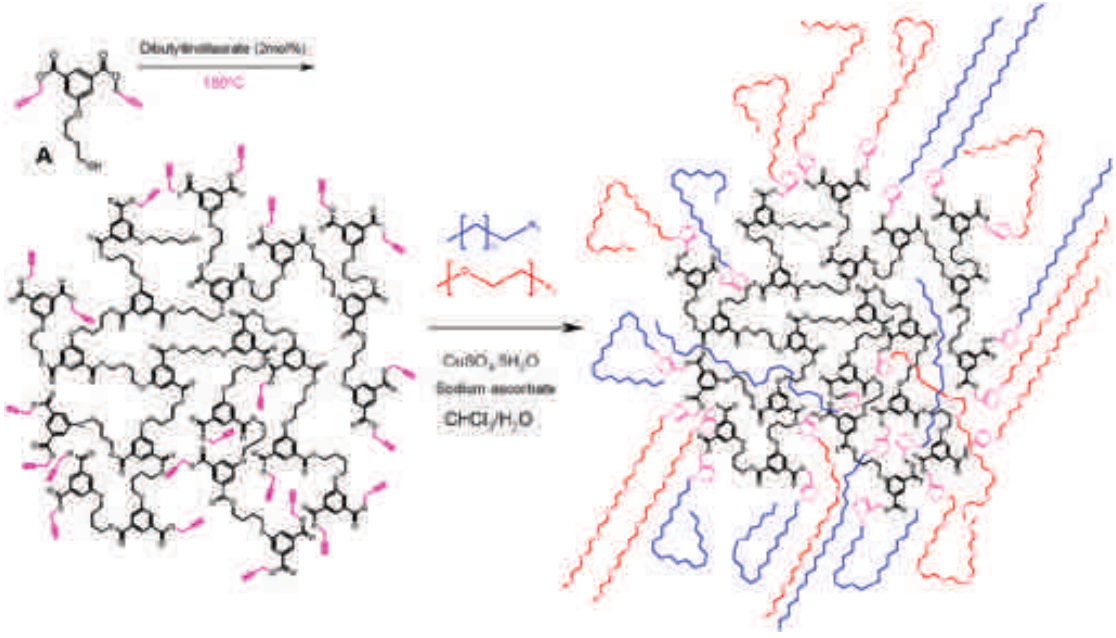

dx.doi.org/10.1021/ma2022277 | *Macromolecules* 2012, 45, 2348−2358

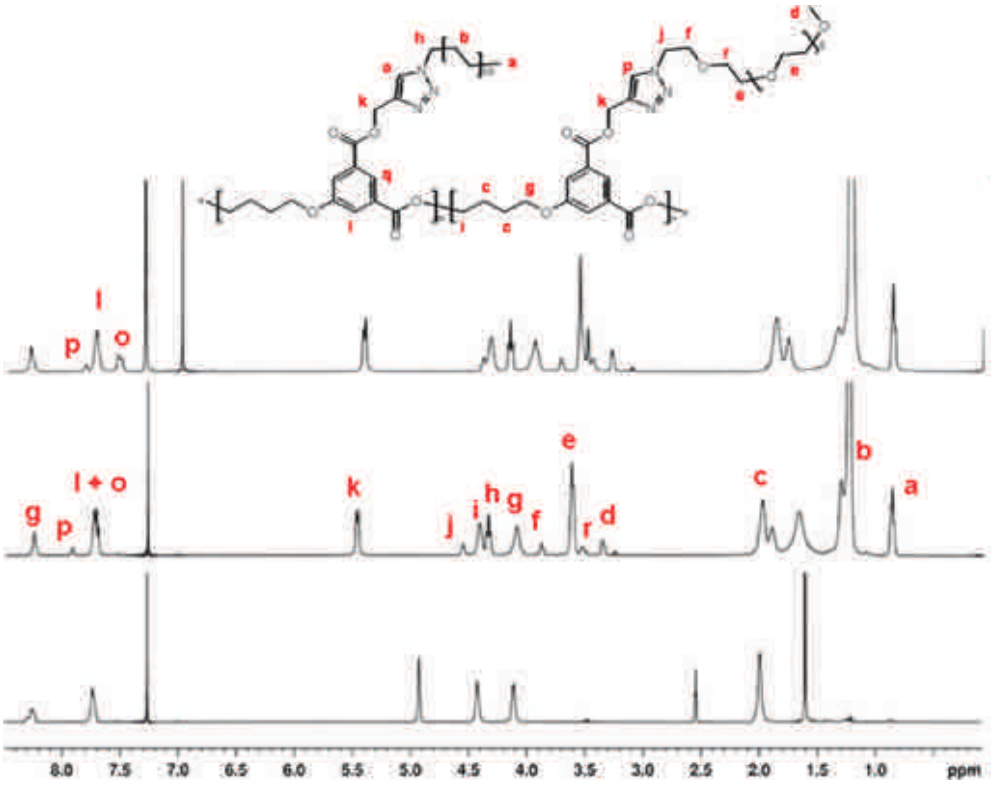

Figure 1. ^{1}H NMR spectra of parent HBP-PE (bottom), DOCOPEG-7030 in $CDCl_3$ (middle), and in $CDCl_3$ + C_6D_6 (top); use of a solvent mixture helped resolve the peaks l and o, the ratio of which was used as an internal consistency check of the percentage incorporation of docosyl azide and PEG (350) azide. Complete disappearance of propargyl peaks, at 4.9 and 2.6 ppm, demonstrates the efficacy of click reaction.

Table 1

	percentage incorporation from NMR		percentage feed					
name	docosanol	PEG	docosanol	PEG	mol wt (M_w) (g/mol)	PDI	enthalpy of melting (J/g)[a]	mp (°C)
parent HBP					84 000	15		
DOCOPEG-3070	34	66	30	70	35 400	2.5	120[c]	50[d]
DOCOPEG-5050	56	44	50	50	39 900	2.9	146	57
DOCOPEG-7030	81	19	70	30	145 600	8.8[b]	147	61

[a]Enthalpy values were taken from the heating curves and were normalized with respect to the wt % of docosyl segments in the HBP. [b]Possibly due to aggregation. [c]Estimated during the cooling curve, as the melting endotherm was very broad. [d]The endotherm was very broad and hence this value is not very accurate (see Figure S15).

around 0.9 and 3.4 ppm (peaks a and d), respectively, are well-resolved, and therefore, their intensities were directly employed to estimate the extent of their incorporation in the HBP. Furthermore, recording the spectrum in the presence of C_6D_6 permitted the resolution of peaks due to the triazole ring proton that belongs to docosyl and PEG units (peaks marked p and o);[32] the intensities of these protons could also be used to estimate the relative composition of the two units in the final clicked polymer. The composition obtained from both these methods match well and thus helps reconfirm the peak assignments. Similarly, the composition of the other two HB polyesters, clicked with different mole ratios of the docosyl and PEG units, namely 50/50 and 30/70, were also estimated based on their NMR spectra (Figure S1). The composition of the HBPs varies in reasonable accordance with the feed composition as evident from Table 1, although the incorporation of the docosyl unit is consistently slightly higher in all cases. The molecular weights of the parent HBP and the amphiphilic derivatives were estimated by GPC (Figure S2), and the values obtained have been listed in Table 1; the parent polymer as stated earlier had a very broad molecular weight distribution; however, upon derivatization the polydispersity index (PDI) decreased substantially in two cases, while in DOCOPEG-7030 a very broad distribution was seen. The reduction in PDI in two cases could either reflect the inherent insensitivity of the hydrodynamic volumes of such peripherally functionalized HBPs to molecular weight variations and/or could be due to fractionation that could have occurred during the purification of the postfunctionalized polymers. In the case of DOCOPEG-7030, although a similar procedure of isolation was used, the PDI continues to be high; this may be due to some aggregation, even though at this time we have no direct evidence for such aggregation.

Thermal Studies. One of the reasons for choosing the docosyl unit was to exploit the strong tendency of these long-chain alkyl segments to crystallize, which in turn would provide an added motivation for intrachain self-segregation. The simplest way to study phase separation is to examine the DSC curves of the

dx.doi.org/10.1021/ma2022277 | *Macromolecules* 2012, 45, 2348−2358

peripherally functionalized HBPs. In Figure 2, both the heating and cooling DSC curves of the three samples are presented; it is

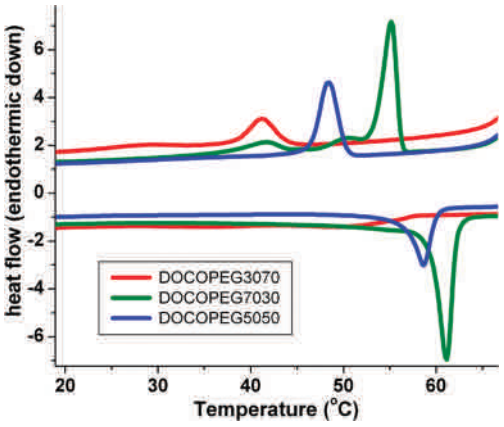

Figure 2. DSC curves (heating and cooling) of the DOCOPEG-*xy* polymers, showing clear melting and crystallization peaks. The melting transition of DOCOPEG-3070 appears as a very broad peak, while the crystallization exotherm during the cooling is sharper.

evident that the two samples having the higher mole fraction of docosyl units exhibit a clear melting peak during the heating scan, while DOCOPEG-3070 exhibits a very broad peak during the heating scan, although the crystallization exotherm during the cooling scan is sharper. The presence of this clear endothermic peak is ascribed to the melting of the docosyl segment,[33] and it provides the first evidence for the ability of the hyperbranched core to reorganize and permit segregation of the randomly placed peripheral PEG and docosyl segments. The DSC curves also reveal some other interesting trends: (a) both T_m and T_c and their associated enthalpies are seen to vary with the composition, and (b) the extent of supercooling is seen to change with composition. In order to compare the melting enthalpies, they should be normalized with respect to the docosyl content in the polymer; the normalized enthalpy values thus obtained for the three HBPs are listed in Table 1. Since the peak has been ascribed to the melting of the crystalline domains formed by the docosyl segments, one would expect the melting temperature and the normalized enthalpies to remain invariant with composition; however, as evident from Table 1, the T_m decreases with the docosyl composition. The ΔH_m values, however, are nearly the same for DOCOPEG-7030 and -5050 but substantially smaller for DOCOPEG-3070. This suggests that the phase separation in the former two samples is fairly complete, while this may not be the case when the PEG content is very high, thereby causing the melting peak to broaden out considerably, and this also causes the enthalpy value to decrease. The DSC thermograms of the hyperbranched polymers containing only docosyl or PEG units were also recorded; DOCO-100 exhibited a clear melting peak (normalized ΔH_m was ~136 mJ/mg; see Figure S-13), while the PEGylated HBP was completely amorphous (Figure S-14). The slightly lower value of normalized melting enthalpy of DOCO-100 probably reflects the larger mismatch in solubility parameters in the DOCOPEG-*xy* polymers, leading to more effective phase separation. It may be relevant to recall that the enthalpy of melting of a long-chain hydrocarbon of a similar size has been reported to be around 157 mJ/mg,[34] which is clearly in the vicinity of those seen for the higher docosyl-containing samples.

Studies at the Air–Water Interface. It is well-known that amphiphilic molecules and block copolymers demonstrate a strong tendency to orient themselves at the air–water interface with the polar segments solvated in water;[35,36] the spreading behavior of such systems is typically evaluated by measuring the surface pressure–area isotherms (π–A diagram) using a Langmuir trough. Langmuir isotherms have been effectively used in the past to clearly demonstrate the conformational adaptability of core–shell type PAMAM dendrimers[37] and hyperbranched polyesters[38] wherein the polar core was shown to flatten out and spread at the water surface pushing the long-chain alkylene peripheral groups upward. In the case of our randomly functionalized hyperbranched DOCOPEGs, the π–A isotherms will serve to probe the ability of randomly amphiphilic structures to reconfigure to Janus-type ones.

The π–A isotherms of the three different HBPs are shown in Figure 3; two distinctive features of DOCOPEG-7030 are the

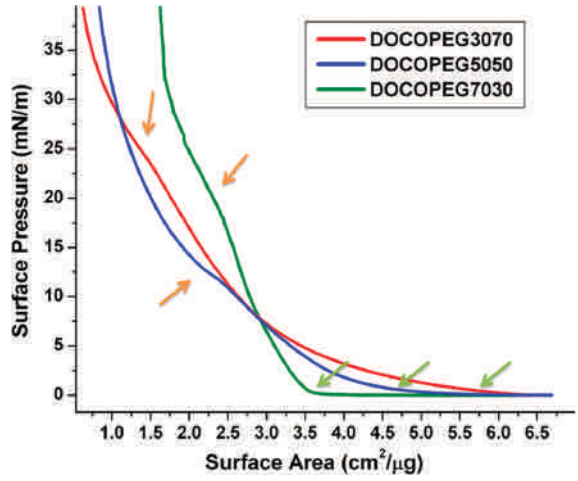

Figure 3. Langmuir isotherms for DOCOPEG-7030 (green), DOCOPEG-5050 (blue), and DOCOPEG-3070 (red); the green arrows indicate the points at which the surface pressure begins to increase, while the orange arrows mark the break in the curve, indicating a slight densification. The surface area has been normalized with respect to the weight of the polymer sample added to the interface.

sharpness in the rise of the surface pressure during compression and the area at which this rise begins. Another important aspect is the break in the slope of the curve during the compression (indicated by the orange arrow); this inflection occurs at different surface pressures for the different HBPs. These observations, taken together with the earlier DSC data, suggest that the inflection in the π–A isotherms could reflect a pseudocrystallization associated with the docosyl chains, which would lead to a densification of the alkylene segments at the air–water interface and cause a reduction in surface pressure; under experimental conditions where the area is being continuously reduced, this would be reflected as a change in slope. Earlier studies using simple surfactants,[39,40] as well as amphiphilic polymers,[41] have also exhibited a similar change in the slope. In the case of simple surfactants one often observes a plateau while in the case of the polymers it appears as a break in the slope; this has been ascribed to a fluid–gel phase transition of the long-chain alkyl segments. As the composition of the HBPs is varied, the volume fraction occupied by the docosyl segment decreases and therefore the surface area at which the inflection occurs also decreases, as seen in the figure. The structural ramification of the inflection is also revealed by

dx.doi.org/10.1021/ma2022277 | *Macromolecules* 2012, 45, 2348–2358

examining the hysteresis in the $\pi-A$ isotherms; the break in the curve is not seen during the decompression segment (Figure S3). This suggests the presence of residual densely packed islands during the decompression, which disintegrates very slowly only at much lower surface pressures. The presence of such islands is also revealed in the interesting aggregate structures that are seen in the AFM images of monolayers transferred onto silicon substrates, as will be discussed later. One other difference in behavior of DOCOPEG-7030 is that there is a continuous change in the isotherm with the cycling, although in the other two samples the isotherms are perfectly reproducible (Figure S4). We presently do not completely understand the origin of this difference; the possibility of sample dissolution was, however, discounted by control experiments using a prewashed sample. Furthermore, of the three samples, DOCOPEG-7030 has the lowest solubility in water which further weakens this possible explanation.

Further evidence for the pseudocrystallization of the docosyl segments comes from quasi-static studies; here, at different points of the isotherm, the compression was stopped and the surface pressure was monitored as a function of time. A drop in surface pressure at constant area is a clear indication of densification. The results of such experiments are shown in Figure S5; the sawtoothed curve represents the drop in surface pressure seen at different points along the quasi-static isotherms. In order to obtain a relative estimate of the extent of this pressure drop, the quasi-static experiments were carried out at a single point (after the inflection point) during the compression (Figure 4); the

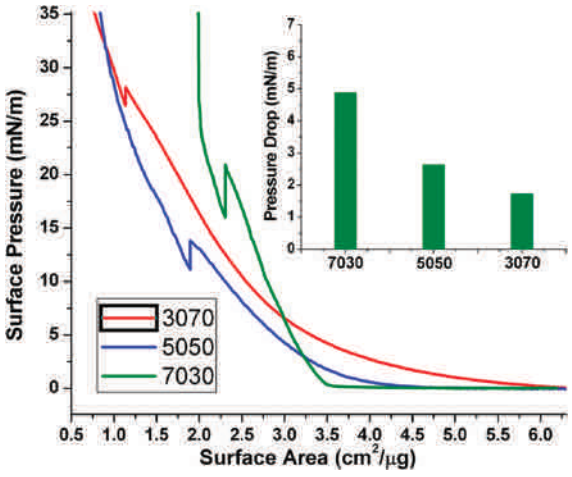

Figure 4. Langmuir isotherms of the three HBPs during a two-step quasi-static compression. The pressure drop (inset) is largest for DOCOPEG-7030, which has the highest docosyl content. The surface area has been normalized with respect to the weight of the polymer sample added to the interface.

duration for which the pressure drop was monitored was fixed (~10 min) to ensure that maximum drop had been attained (see Figures S6 and S7). The magnitude of this pressure drop would be proportional to the extent of densification; the inset in Figure 4 clearly reveals that this drop is highest in the case of DOCOPEG-7030, as expected, and it decreased with decrease in docosyl content. These experiments again clearly demonstrate these randomly amphiphilic HBPs do reconfigure at the air−water interface to generate Janus structure.

Atomic Force Microscopic Studies. In order to visualize the state of molecular aggregation during the compression at the air−water interface, the monolayer was transferred onto a hydrophilic (piranha-treated) silicon wafer; in each case this was done at two different surface pressures—one at a high value just before the collapse of monolayer and the other at a point immediately following the inflection in the isotherm. The AFM images of the three samples at the two different surface pressures are shown in Figure 5. At the higher surface pressure, the samples with higher PEG content (3070 and 5050) appear to form fairly uniform films; the average film thickness was estimated to be around ~3 nm, as measured by the depth of the holes in the film. On the other hand, DOCOPEG-7030 exhibited incomplete coverage, and the average film thickness was slightly lower at ~2.5 nm. Interestingly, at lower surface pressures, the two higher PEG samples exhibit uniform elongated bundles (height ~2.0−2.5 nm; single bundle width ~44 nm); this suggests that some type of clustering to form islands may be occurring on the air−water interface due to the interaction between the docosyl segments, and these islands get transferred (see Figure S8 for a schematic depiction of this process) onto the substrate during the formation of the LB films. Similar observations of dendritic aggregate structures at the air−water interface were earlier made in the case of simple surfactants; direct fluorescence microscopic observations of dye-stained samples revealed that such structures are already formed at the air−water interface.[42] Such structures were, however, not seen in the case of DOCOPEG-7030; this observation evades a simple explanation. It is also interesting to note that the lengths of elongated bundles are significantly smaller in DOCOPEG-3070, while the heights in both cases are similar and correspond roughly to the monolayer thickness.

Model for Interfacial Behavior of Amphiphilic HBPs. From the above observations it is clear that randomly clicked HBPs, bearing varying amounts of the hydrophilic (PEG) and hydrophobic (docosyl) segments at their molecular periphery, can exhibit Janus-type behavior by conformational reorganization of the hyperbranched polymer backbone. This leads to the typical amphiphilic behavior at the air−water interface, as evident from the Langmuir isotherms. However, to further understand the subtle nuances of the $\pi-A$ isotherms, one needs to take into account the relative volume fractions of the hydrophobic and hydrophilic segments; a simplistic model representation of the HBPs with three different compositions is shown in Scheme 2. Depending on the relative volume fractions of the docosyl, PEG, and the HB polymer backbone, several possible scenarios can arise during the compression at the air−water interface (Scheme 2): (a) the volume and projected surface area of the solvated PEG chains in the aqueous subphase is larger than that of the docosyl segments, (b) these are roughly of similar magnitude, and (c) the docosyl segments occupy larger volume that the PEG units. Thus, during the compression the first contact between individual macromolecules could occur either in the subphase between the PEG chains or above the interface between the docosyl units. In DOCOPEG-7030, it appears that the contact occurs above the air−water interface; a rapid rise in surface pressure is noted as the area is reduced. Beyond a certain surface pressure the docosyl chains appear to go into an ordered 2D lattice that leads to a more efficient packing, and hence a densification occurs; this causes a slight change in the slope during the compression and is also the reason for the considerable drop in surface pressure upon prolonged holding at a constant area, as seen in the quasi-static measurement. On the other hand, in both the other polymers, namely DOCOPEG-5050 and

dx.doi.org/10.1021/ma2022277 | Macromolecules 2012, 45, 2348−2358

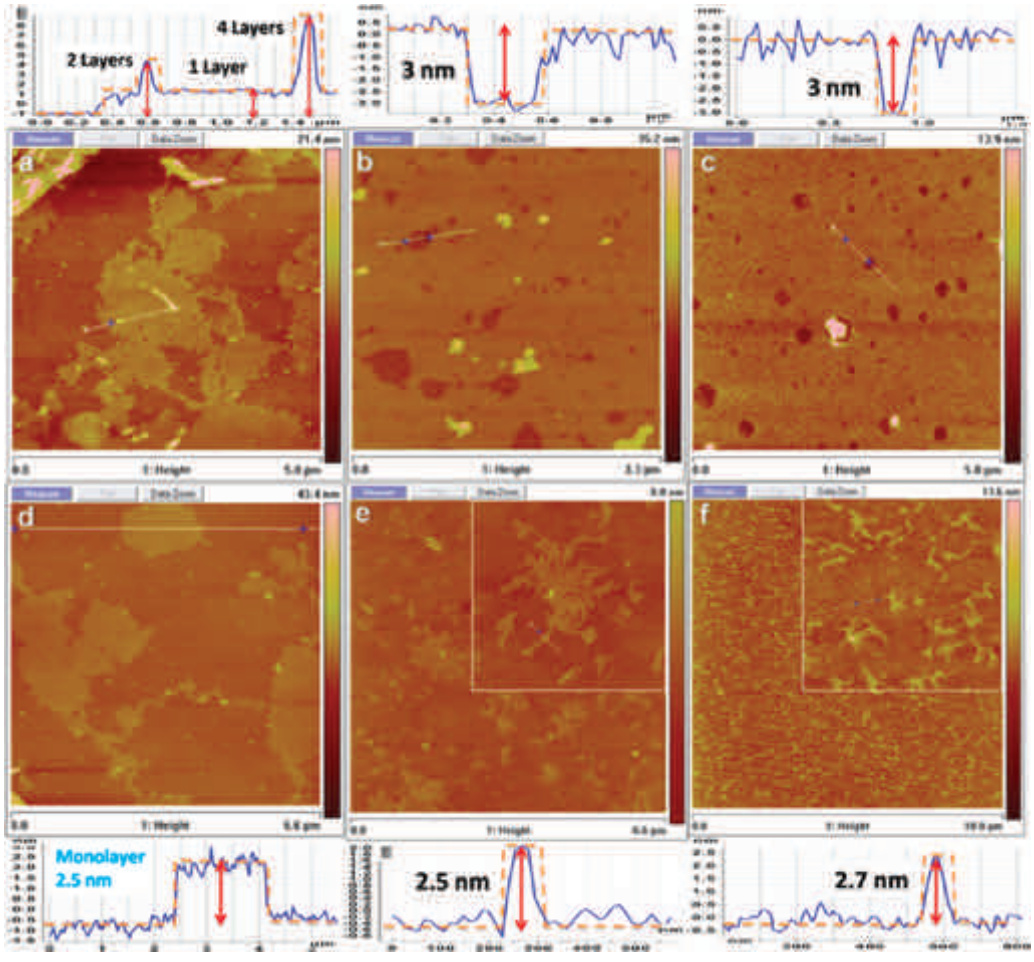

Figure 5. AFM images of monolayers transferred onto hydrophilic silicon wafer: images a, b, and c are a monolayer of DOCOPEG-7030, -5050, and -3070, respectively, transferred at a surface pressures of ∼35 mN/m, while images d, e, and f represent those transferred at a surface pressure slightly above the respective inflection points for each sample.

Scheme 2. A Pictorial Representation of Possible Events during the Compression of the Amphiphilic Janus HBPs at the Air–Water Interface[a]

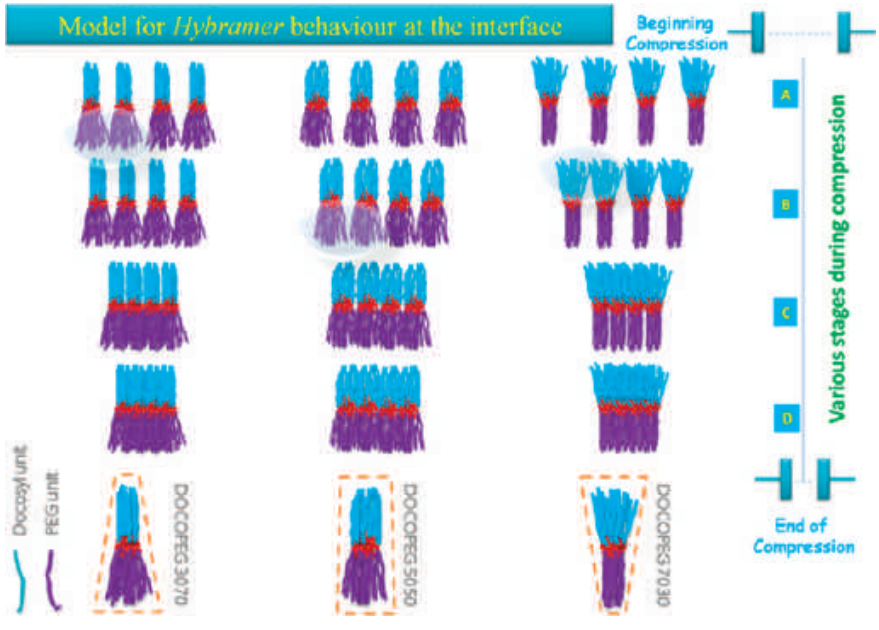

[a]The points of first contact between the chains for the polymers are highlighted.

dx.doi.org/10.1021/ma2022277 | *Macromolecules* 2012, 45, 2348–2358

DOCOPEG-3070, one notices that the change in surface pressure during compression is much more gradual and occurs at much larger surface areas. This is interpreted as being due to the fact that the first contact between molecules may be occurring in the aqueous subphase between the solvated PEG chains; the significantly higher conformational flexibility (*softer*) of these PEG chains leads to the significantly slower rise in the surface pressure at the early stages. Beyond a certain compression, the docosyl chains come in contact, and a similar densification due to pseudocrystallization causes the kink in the isotherm; the point at which this happens is evidently dependent on the relative volume fraction of the docosyl segments. Thus, the area at which this kink occurs would be roughly proportional to the relative volume fraction of the docosyl segments, as seen in the isotherms. A schematic depiction of these events at the air−water interface is presented in Scheme 2; further detailed calculations of the relative volumes of the hydrophobic and hydrophilic (solvated) segments would be required to strengthen this hypothesis.

SAXS Studies of Bulk Samples. DSC studies of the three HBPs clearly revealed that the docosyl segments self-segregate and crystallize independently. In order to gain a better understanding of the bulk morphology of these HBPs, we carried out small-angle X-ray scattering (SAXS) measurements. Prior to studying the amphiphilic systems, we examined the HBP that contains only docosyl chains at their periphery, as this would also help address the question of conformational adaptability of the hyperbranched core to permit the peripheral alkyl segments to segregate and organize in a crystalline lattice. Similar studies on peripherally alkylated PPI dendrimers were reported earlier by Meijer and co-workers;[43] they had suggested the formation of lamellar morphology wherein the dendrimers adopt a jellyfish-like conformation. The SAXS data of completely alkylated polymer (DOCO100) are shown in Figure 6. A typical lamellar pattern is evident, suggesting a

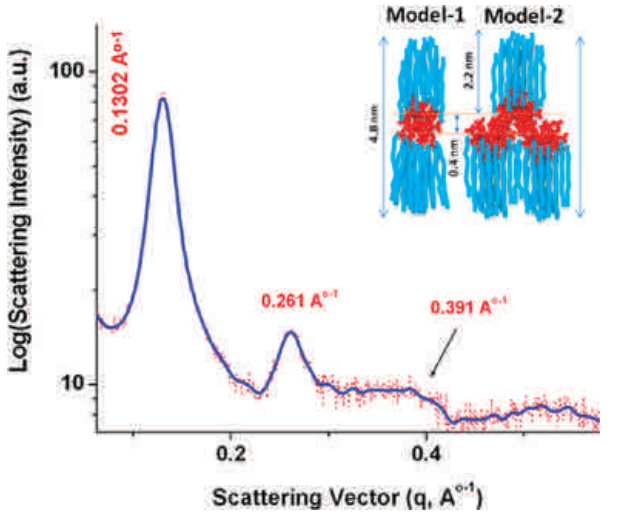

Figure 6. SAXS pattern observed for DOCO-100; the peak positions were in the ratio 1:2:3, confirming the lamellar morphology. A pictorial depiction of the two possible models is shown in the inset; the SAXS data do not permit the discrimination between these two possibilities.

lamellar thickness of 4.8 nm; based on the model by Meijer, this spacing could be explained by two possible molecular arrangements, as shown in the figure. The spacing obtained here matches reasonably well with those seen in alkylated poly(propyleneimine) dendrimer carrying 16 terminal alkyl units.[43] On the basis of an all-trans conformation of the docosyl unit, which would give a length of about 2.2 nm, a rough estimate of the expected lamellar thickness can be readily made; two of the docosyl segments within a lamella would roughly account for about 4.4 nm implying that the HBP backbone roughly adds only about 0.4 nm, suggesting a fairly compact and flattened conformation.

The SAXS patterns of the three amphiphilic HBPs clearly revealed their strong tendency to form lamellar morphologies; DOCOPEG-7030 and DOCOPEG-5050 exhibited a higher degree of ordering. The SAXS profiles of three polymers are shown in Figure 7; in all cases the polymers were melted and

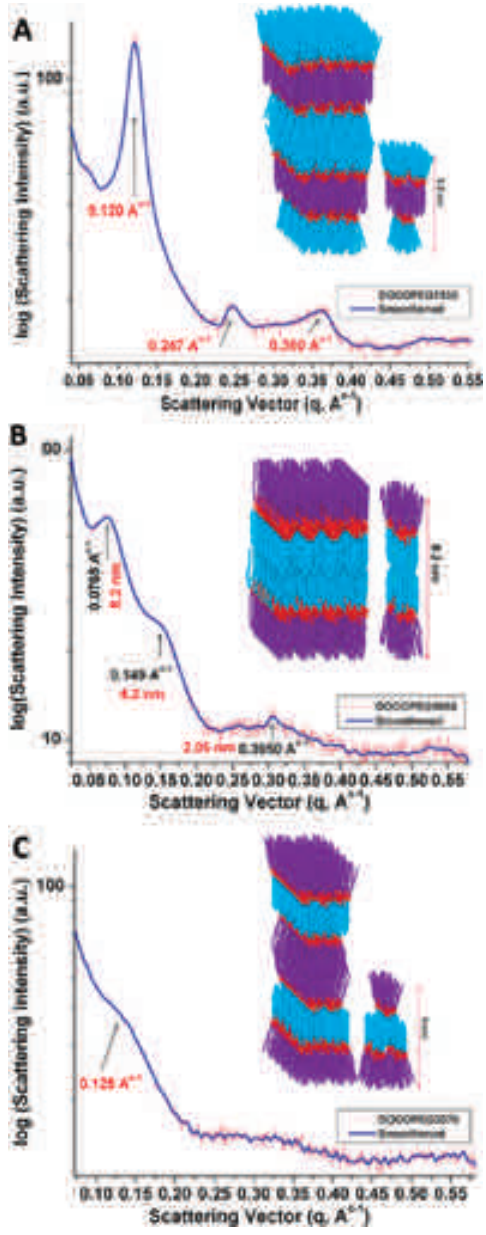

Figure 7. SAXS pattern observed in the case of DOCOPEG-7030 (A), DOCOPEG-5050 (B), and DOCOPEG-3070 (C). The peak positions are in the ratio 1:2:3, confirming the lamellar morphology.

short fibers were pulled and used for the experiments (the waxy samples readily permitted pulling short fibers from the melt by simply using a capilliary). In the two samples with higher docosyl content, several higher order scattering peaks are

dx.doi.org/10.1021/ma2022277 | *Macromolecules* 2012, 45, 2348−2358

clearly visible; this suggests the formation of highly ordered structures. Interestingly, the treatment of the samples with hot water lead to a substantial improvement in the sharpness of the scattering peaks, suggesting a solvent-induced annealing process; however, in this case the solvent probably improves the phase separation by diffusing into the PEG domains, leading to a more effective compaction of the paraffinic domains (Figure S9). While the fibers permitted easy handling of the samples, this could also induce some alignment; in order to check this we carried out the SAXS measurement of a solid sample of DOCOPEG-5050 (Figure S10), precipitated out of methanol. The pristine untreated sample also exhibited peaks at nearly identical positions, suggesting the formation of lamellar morphology even in as-precipitated samples; this confirmed the strong tendency for intrachain phase separation in these HBPs that is facilitated by the readaptation of the polymer backbone to permit the self-segregation of the docosyl and PEG chains.

The *d*-spacing retrieved from the SAXS data of the three HBPs reveal some very interesting insights into the possible molecular ordering in these systems; the lamellar spacing is about 8.2 nm in the case of DOCOPEG-5050, while it is only 5.2 and 5.0 nm in the case of DOCOPEG-7030 and DOCOPEG-3070, respectively. This suggests that when the relative volumes of the docosyl and PEG segments are comparable, as in DOCOPEG-5050, there is little interdigitation and the spacing reflects the dimension of the self-segregated HBP. While in the other cases wherein the relative volume fractions of either docosyl or PEG segments are significantly smaller, there is considerable interdigitation to achieve complete volume filling which causes the lamellar spacing to reduce considerably; a schematic depiction of this ordering is presented in Figure 7 (inset). In DOCOPEG-3070, the phase separation is less pronounced possibly because the added motivation for phase separation, which is the strong tendency for the docosyl segments to crystallize, is less pronounced in this case; this contention is also supported by the DSC data.

In a final experiment, SAXS studies were carried out as a function of sample temperature in the case of DOCOPEG-5050; the SAXS patterns of the sample below and above the melting point of the docosyl segments are shown in Figure 8.

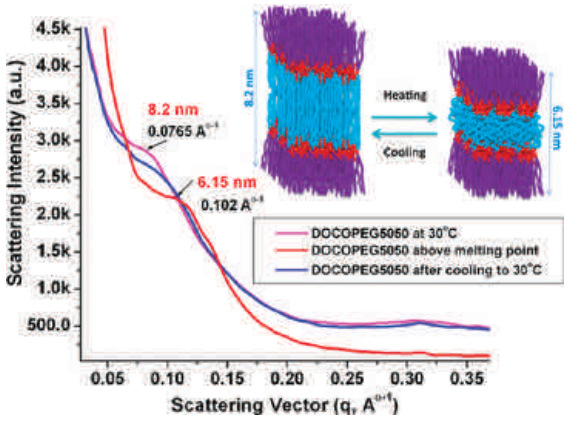

Figure 8. SAXS data of DOCOPEG-5050 sample reprecipitated from methanol. Effect of thermal cycling causes reversible melting and recrystallization of docosanol domains and which is reflected in the SAXS peak shift. The data after melting (red line) are *y*-scaled for clarity.

It is evident that there is a shift of the peak to higher *q* values at a temperature above the melting point of the docosyl segments; this is a clear indication of melting and consequent shrinking of the hydrocarbon domains causing the lamellar spacing to reduce to 6.15 nm. Interestingly, upon cooling the SAXS pattern reverts back to nearly its original form, indicating that recrystallization of the docosyl segments leads to near complete recovery of the original lamellar structure.

Self-Assembly of *Janus HBPs* in Solution. Just as traditional amphiphiles, these Janus HBPs may also form aggregates in solution under suitable conditions. In order to probe this, a chloroform solution of DOCOPEG-7030 was added into methanol, which is a selective solvent for PEG segments alone; this lead to a light-blue scattering solution indicating aggregate formation. AFM images of the aggregates revealed the existence of uniform flat disklike aggregates of height ~5 nm, which roughly corresponds to a bilayer (recall that the monolayer thickness was around 2.5 nm); the proposed structure of these disklike aggregates is shown in Figure 9, wherein the PEG units sandwich the central domains formed by the docosyl segments, thereby minimizing their exposure to the polar medium. In the case of DOCOPEG-5050, the aggregates do not form immediately; however, a light blue scattering solution is formed only upon prolonged aging (~2 weeks) (Figure S11). In the case of DOCOPEG-3070, however, no aggregates are formed evidently due to its higher solubility in a polar solvent, like methanol. The formation of these aggregates is clearly driven by the desire to minimize contact between the hydrophobic docosyl segments and the polar medium and is further stabilized by the tendency for the docosyl segments to crystallize. Apart from generating aggregates, we also attempted to prepare vesicles using the standard hydration protocol;[44] it was observed that DOCOPEG-3070 formed exclusively vesicles of fairly uniform size (Figure 10), while in the case of DOCOPEG-5050 both vesicles and disklike aggregates are seen. As evident from the AFM and TEM images, the height of the vesicles (deflated upon deposition) roughly corresponded to twice the bilayer thickness, as expected; similarly, a rough estimate of vesicle wall thickness from the TEM was found to be ~5 nm (Figure S12), which also agrees with bilayer thickness estimated from SAXS studies. DOCOPEG-7030 did not form vesicles; attempts to do so simply resulted in the formation of a macroscopic precipitate. On the basis of simple geometric arguments put forward by Israelachvili,[45] the relative volumes of the hydrophobic and hydrophilic segments would govern the nature of the aggregates formed; for vesicles the projected areas of these segments must be roughly equal. Hence, on the basis of our observations, it appears that DOCOPEG-3070 best meets this criteria followed by DOCOPEG-5050. Evidently, the interdigitation of the docosyl segment and the curvature of the vesicle membrane together appear to most favor the formation of vesicles in the case of DOCOPEG-3070.

One feature common to all the amphiphilic HBPs examined in this study is their highly polydisperse nature; it may, therefore, be pertinent to reflect on the possible influence of such broad molecular weight distribution on the properties that have been examined. Considering the structural adaptability of the relatively small hyperbranched backbone (typical DP ~ 20), it may be reasonable to view the Janus structure as a cluster of nonionic surfactants stitched together at the center by the HBP backbone. The polydispersity of the sample would primarily affect its DP value, and consequently it will amount to varying the number of surfactants bundled together to form the Janus structure. It may, therefore, be expected that most of the properties that have been presented in this study, namely melting

dx.doi.org/10.1021/ma2022277 | *Macromolecules* 2012, 45, 2348–2358

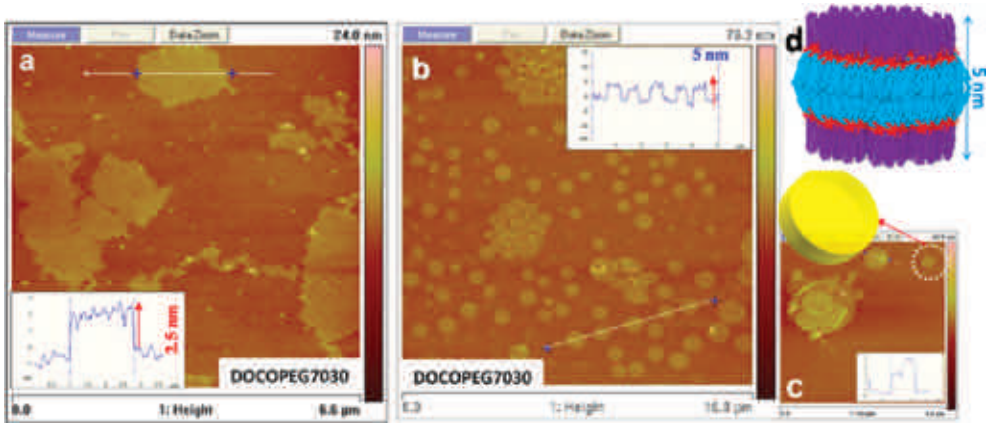

Figure 9. (a) AFM image of the monolayer from LB studies (DOCOPEG-7030); (b) self-assembled bilayer disk obtained from methanol (DOCOPEG); (c) multilayered deposition of the disks formed in methanol; and (d) proposed model structure of the bilayer.

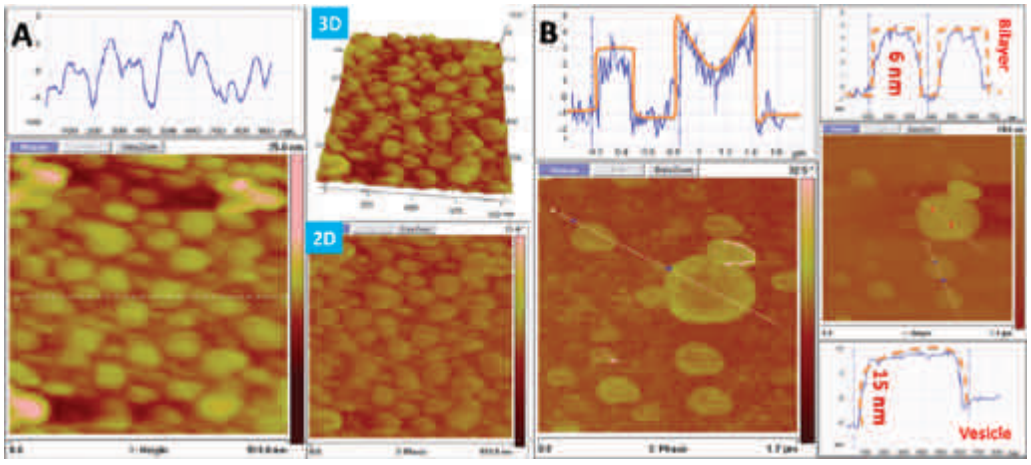

Figure 10. AFM images of vesicles obtained from (A) DOCOPEG-3070 and (B) DOCOPEG-5050. DOCOPEG-3070 forms exclusively vesicles while DOCOPEG-5050 forms vesicles (curved line profile) and bilayer disks (flat line profile). Since the center of vesicle is relatively flexible than the edges, line profile of the phase image shows a dip at the center of the vesicle, while the bilayer disks shows a flat line profile. (More TEM and AFM images are available in the Supporting Information, Figures S11 and S12.)

enthalpies, lamellar spacing, etc., are not likely to be affected by the polydispersity of the samples. Although this structural analogy may be strictly applicable only to DOCOPEG-5050, arguments along similar directions would suggest that the polydisperse nature of all these amphiphilic HBPs will have minimal effect on the properties examined.

In conclusion, we have shown that peripherally clickable hyperbranched polyesters can be readily functionalized using the azide−yne click reaction to generate a range of amphiphilic systems, wherein the relative mole fractions of the long-chain hydrocarbon segment (C22-docosyl) and PEG (PEG300-monomethyl ether) can be varied. Although the click reaction of the peripheral propargyl groups would lead to a random placement of the docosyl and PEG units, *we have demonstrated unequivocally that the hyperbranched polymer backbone reconfigures to permit the self-segregation of the docosyl and PEG segments to form Janus-type structures.* DSC studies clearly revealed a transition corresponding to the melting of the crystalline domains formed by the docosyl segments, the enthalpy of which varied in proportion to the docosyl content. Langmuir isotherms of these amphiphilic HBPs showed several interesting features that again confirmed the ability for these systems to reconfigure into Janus-type structures; importantly, we see evidence for densification due to pseudocrystallization of the docosyl segments above a threshold surface pressure; the extent of densification was again proportional to the volume fraction of the docosyl units. The nature of the aggregates formed upon precipitation of a dilute solution of the polymers into methanol was also examined. AFM studies clearly revealed the formation of disklike aggregates whose heights suggested the formation of bilayers containing docosyl segments in the center with PEG segments on either side; these segments, in a sense, encapsulate the hydrophobic domains from the polar solvent. DOCOPEG-3070 formed fairly uniform vesicles under standard hydration protocol, which was confirmed both by AFM and TEM studies. Finally, SAXS investigations clearly reveal the formation of lamellar morphology, providing further evidence for the self-segregation of the docosyl and PEG units. Interestingly, the lamellar spacing also suggests that molecular organization depends strongly on the relative volume fractions of the docosyl and PEG segments; a high level of interdigitation appears to occur when the volume fraction of either of these segments are small, causing a shrinkage in the lamellar spacing, but when their volumes are roughly similar, the spacing is significantly larger. *In summary, these investigations clearly demonstrate for the first time that structural perfection in placement of the hydrophilic and hydrophobic entities, such as those present in Janus Dendrimers, is not essential for eliciting*

dx.doi.org/10.1021/ma2022277 | *Macromolecules* 2012, 45, 2348−2358

Janus-type properties. The conformational flexibility of the hyperbranched polymers permits reconfiguration of the polymer backbone to generate Janus-type structures; if there is adequate thermodynamic motivation, which in the present systems are immiscibility of the docosyl and PEG segments and the strong tendency for the docosyl segments to crystallize, then the self-segregated structures formed could be further stabilized. These self-adapting Janus-type hyperbranched structures, which we have termed *Janus hybramers*, could serve as useful scaffolds for further derivatization and thereby permit strategic placement of a variety of function-performing entities with a controllable periodicity.

EXPERIMENTAL SECTION

Materials and Methods. All the solvents used for synthesis were purified prior to use following standard procedures. 5-Hydroxyisophthalic acid, 1,2-dibromoethylene, magnesium turnings, propargyl alcohol, dicyclohexylcarbodiimide (DCC), (*N*,*N*-dimethylamino)-pyridine (DMAP), PEG-350, monomethyl ether, docosonol, tosyl chloride, and sodium azide were purchased from Aldrich Chemical Co. The ^{1}H NMR spectra were recorded using a Bruker AV 400 MHz spectrometer in suitable deuterated solvents using tetramethylsilane (TMS) as internal reference. GPC measurements were carried out using Viscotek triple detector analyzer (TDA) model 300 system, which has a refractive index (RI), a differential viscometer (DV), and light scattering (LS) detectors connected in series. The separation was achieved using a series of two PL gel mixed bed columns (300 × 7.5 mm) operated at 30 °C using THF as the eluent. Molecular weights were determined using a universal calibration curve based on the data from the RI and DV detectors using narrow polystyrene standards. The thermal analysis was performed using a Mettler Toledo DSC instrument at a heating rate of 10 °C/min under a dry N_2 atmosphere. Typically, 2−3 mg of the sample was first heated to a temperature above its melting (to ensure that the sample flows and makes the contact with the pan) and then cooled; two subsequent heating and cooling runs were conducted to ensure reproducibility. Since the melting transitions primarily reflect the melting of the docosyl segments, the enthalpies associated with these transitions were normalized with respect to the weight percent of docosyl segments in the sample, which in turn was estimated from the copolymer composition using NMR.

Click Reaction. The parent hyperbranched polyester was synthesized following the procedure reported earlier.[29] 100 mg (0.36 mmol of peripheral propargyl units) of the parent HB polyester was dissolved in THF and purged with dry N_2 gas. 64.13 mg of docosyl azide (0.18 mmol) and the PEG azide 68.4 mg (0.18 mmol) were added into it. $CuSO_4{\cdot}5H_2O$ (4.66 mg, 0.018 mmol) and sodium ascorbate (7.17 mg, 0.0364 mmol) were separately dissolved in a small amount of water and added into the reaction mixture. After degassing, the mixture was stirred at 50 °C for 3 days. Later, the reaction mixture was concentrated and precipitated into methanol to get white polymer product (DOCOPEG-5050). Similarly, by varying the composition of docosyl azide and PEG-azide, DOCOPEG-7030 and DOCOPEG-3070 were also prepared. DOCOPEG-3070 was reprecipitated in petroleum ether. The yields of the polymers DOCOPEG-7030, DOCOPEG-5050, and DOCOPEG-3070 were 88, 80, and 75%, respectively. Although it was possible to retrieve the dissolved fraction by concentrating the solvent layer, it was not used for further study.

Langmuir−Blodgett (LB) and AFM Measurements. LB studies of DOCOPEG-*xy* were performed using NIMA 1232D1D2 Langmuir−Blodgett trough. Polymer solutions (0.5 mg/mL) were prepared in $CHCl_3$ (HPLC grade), 150 μL of which was spread on the trough. It was found that 150 μL at 0.5 mg/mL of the polymer sample was optimum for generating good monolayer; at higher concentrations aggregation at the interface was seen to occur. Compression experiments were performed at a rate of 50 cm^2/min, and the isocycles were recorded at a rate of 300 cm^2/min. The plots are normalized with respect to the weight of polymer sample delivered on to the air−water interface. The rate of compression for quasi-static compression experiment was 100 cm^2/min. Compressed monolayer was transferred onto a solid substrate at a rate of 1 mm/min. Piranha-treated silicon wafer was used as solid substrate. Quasi-static compression experiments were performed at steps of 20 cm^2 (compression) for DOCOPEG-5050 and at 10 cm^2 for other two samples. The waiting time was 3 min for each step in the quasi-static experiments during the multistep QSC experiment (Figure S5). In order to measure the total pressure drop, the monolayer was compressed to an area which corresponds to largest pressure drop point during the multistep QSC curve for each sample. For example, DOCOPEG-5050 was compressed to an area 140 cm^2; this area corresponds to the point of largest pressure drop (0.96 mN/m) in the multistep QSC curve. Waiting time for the single step compression static event was 560 s for DOCOPEG-7030 and 5050, but a 600 s wait time was used for DOCOPEG-3070. A control water isotherm was recorded, and no significant surface pressure was noticed until the barrier is fully closed; such a flat baseline was ensured before beginning the experiment. AFM measurements were performed using MultiMode SPM (Digital Instruments, Santa Barbara, CA) equipped with NanoScope IV A controller. FESP (Veeco) tips of force constant 1−5 N/m and resonance frequency of 75 kHz were used for imaging the sample; measurements were conducted in the tapping mode. Images were analyzed using the software provided with the instrument.

Small-Angle X-ray Scattering (SAXS). SAXS experiments were performed in Hecus S3Micro system with X-ray point-focusing optics (from Xenocs, Grenoble) equipped with PSD using wavelength 1.542 Å. Three different SAXS experiments were performed. Measurements were performed by filling the sample into a small capillary. SAXS pattern of polymer samples (solid) were recorded without any thermal treatment as well as after melting and recrystallization. The scattering data were also recorded for the melt. Aligning of polymer sample was performed in the following way: the samples were taken in a small glass vial and dipped in a water bath maintained above the melting point of the polymer. A glass needle was plunged into the melt and pulled out slowly to draw small fibers of the polymer; as the fiber cooled it solidified. These fibers were then placed on the surface of water (Millipore) maintained at 40−50 °C for about 10−20 min. The fibers were then dried and filled into capillary tubes for recording the SAXS. The scattering was accumulated for 2−3 h for each sample. Completely alkylated derivative of the hybramer (DOCO-100) was similarly aligned and directly used without treatment with water.

Preparation of Vesicle and Disklike Micelles. Vesicles were prepared following standard procedures.[44] 1 mL of the DOCOPEG-*xy* solution in chloroform (1 mg/mL) was taken in a curved bottom vial, and solvent was evaporated slowly under nitrogen purge. The thin film formed at the bottom was dried under vacuum for 2 h. 3−5 mL of distilled water was added and kept overnight at 4 °C for hydration. Then the sample was sonicated for 10 min at 80 °C and immediately cooled down by dipping into ice-cold water. After 5 min, the sample was vortexed for 10 min; the heating−cooling−sonication cycle was repeated several times until a clear solution resulted. 50−100 μL of the sample solution was cast onto a clean piranha-treated silicon wafer, and AFM images were recorded. Flat disklike aggregates were prepared by adding 100 μL of the DOCOPEG-*xy* solution in chloroform (0.5 mg/mL) into methanol (10 mL) with stirring; stirring was continued for an additional 15 min, after which 50−100 μL of the sample solution was cast onto a clean piranha-treated silicon wafer.

ASSOCIATED CONTENT

Supporting Information

Detailed experimental procedures, NMR spectra, GPC curves, Langmuir isotherm cycles, SAXS data, AFM images, and TEM images. This material is available free of charge via the Internet at http://pubs.acs.org.

AUTHOR INFORMATION

Corresponding Author

*E-mail: raman@ipc.iisc.ernet.in.

Notes

The authors declare no competing financial interest.

■ ACKNOWLEDGMENTS

We thank V. A. Raghunathan from Raman Research Institute for the SAXS measurements and S. Sampath for the monolayer studies; many valuable discussions with both of them are gratefully acknowledged. We also thank S. Umapathy for his valuable suggestions and discussions. S.R. thanks the Department of Atomic Energy for the ORI-Award for the period 2006−2011, and A.Z.S. thanks CSIR for a fellowship.

■ REFERENCES

(1) Cohen, J. *Science* **1995**, *267*, 1265−1266.
(2) Haluska, C. K.; Riske, K. A.; Artzner, V. M.; Lehn, J. M.; Lipowsky, R.; Dimova, R. *Proc. Natl. Acad. Sci. U. S. A.* **2006**, *103*, 15841−15846.
(3) Shimizu, T.; Masuda, M.; Minamikawa, H. *Chem. Rev.* **2005**, *105*, 1401−1443.
(4) Kim, H. C.; Park, S. M.; Hinsberg, W. D. *Chem. Rev.* **2010**, *110*, 146−177.
(5) Zeng, F.; Zimmerman, S. C. *Chem. Rev.* **1997**, *97*, 1681−1712.
(6) Zhou, Y.; Yan, D. *Chem. Commun.* **2009**, 1172−1188.
(7) Rosen, B. M.; Wilson, C. J.; Wilson, D. A.; Peterca, M.; Imam, M. R.; Percec, V. *Chem. Rev.* **2009**, *109*, 6275−6540.
(8) Percec, V.; Wilson, D. A.; Leowanawat, P.; Wilson, C. J.; Hughes, A. D.; Kaucher, M. S.; Hammer, D. A.; Levine, D. H.; Kim, A. J.; Bates, F. S.; Davis, K. P.; Lodge, T. P.; Klein, M. L.; DeVane, R. H.; Aqad, E.; Rosen, B. M.; Argintaru, A. O.; Sienkowska, M. J.; Rissanen, K.; Nummelin, S.; Ropponen, J. *Science* **2010**, *328*, 1009−1014.
(9) Erhardt, R.; Bo1ker, A.; Zettl, H.; Kaya, H.; Pyckhout-Hintzen, W.; Krausch, G.; Abetz, V.; Muller, A. H. E. *Macromolecules* **2001**, *34*, 1069−1075.
(10) Xu, H.; Erhardt, R.; Abetz, V.; Muller, A. H. E.; Goedel, W. A. *Langmuir* **2001**, *17*, 6787−6793.
(11) Erhardt, R.; Zhang, M.; Boker, A.; Zettl, H.; Abetz, C.; Frederik, P.; Krausch, G.; Abetz, V.; Muller, A. H. E. *J. Am. Chem. Soc.* **2003**, *125*, 3260−3267.
(12) Walther, A.; Andre, X.; Drechsler, M.; Abetz, V.; Muller, A. H. E. *J. Am. Chem. Soc.* **2007**, *129*, 6187−6198.
(13) Walther, A.; Hoffmann, M.; Muller, A. H. E. *Angew. Chem., Int. Ed.* **2008**, *47*, 711−714.
(14) Walther, A.; Matussek, K.; Muller, A. H. E. *ACS Nano* **2008**, *2*, 1167−1178.
(15) Nierengarten, J. F.; Eckert, J. F.; Rio, Y.; Carreon, M. P.; Gallani, J. L.; Guillon, D. *J. Am. Chem. Soc.* **2001**, *123*, 9743−9748.
(16) Hawker, C. J.; Wooley, K. L.; Frechet, J. M. J. *J. Chem. Soc., Perkin Trans. 1* **1993**, *12*, 1287−1297.
(17) Meyers, S. R.; Juhn, F. S.; Griset, A. P.; Luman, N. R.; Grinstaff, M. W. *J. Am. Chem. Soc.* **2008**, *130*, 14444−14445.
(18) Antoni, P.; Hed, Y.; Nordberg, A.; Nystrom, D.; Holst, H. V.; Hult, A.; Malkoch, M. *Angew. Chem., Int. Ed.* **2009**, *48*, 2126−2130.
(19) Feng, X.; Taton, D.; Ibarboure, E.; Chaikof, E. L.; Gnanou, Y. *J. Am. Chem. Soc.* **2008**, *130*, 11662−11676.
(20) Yan, D.; Zhou, Y.; Hou, J. *Science* **2004**, *303*, 65−67. Zhou, Y.; Yan, D. *Chem. Commun.* **2009**, *10*, 1172−1188.
(21) Sunder, A.; Krämer, M.; Hanselmann, R.; Mülhaupt, R.; Frey, H. *Angew. Chem., Int. Ed.* **1999**, *38*, 3552−3555.
(22) Sunder, A.; Hanselmann, R.; Frey, H.; Mülhaupt, R. *Macromolecules* **1999**, *32*, 4240−4246.
(23) Saha, A.; Ramakrishnan, S. *J. Polym. Sci., Part A: Polym. Chem.* **2009**, *47*, 80−91.
(24) Saha, A.; Ramakrishnan, S. *Macromolecules* **2008**, *41*, 5658−5664.
(25) Ornatska, M.; Peleshanko, S.; Genson, K. L.; Rybak, B.; Bergman, K. N.; Tsukruk, V. V. *J. Am. Chem. Soc.* **2004**, *126*, 9675−9684.
(26) Ornatska, M.; Bergman, K. N.; Goodman, M.; Peleshanko, S.; Shevchenko, V. V.; Tsukruk, V. V. *Polymer* **2006**, *47*, 8137−8146.
(27) Aathimanikandan, S. V.; Savariar, E. N.; Thayumanavan, S. *J. Am. Chem. Soc.* **2005**, *127*, 14922−14929.
(28) Chute, J. A.; Hawker, C. J.; Rasmussen, K. Ø.; Welch, P. M. *Macromolecules* **2011**, *44*, 1046−1052.
(29) Ramkumar, S. G.; Rose, K. A. A.; Ramakrishnan, S. *J. Polym. Sci., Part A: Polym. Chem.* **2010**, *48*, 3200−3208.
(30) Feast, W. J.; Stainton, N. M. *J. Mater. Chem.* **1995**, *5*, 405−411.
(31) Rostovtsev, V. V.; Green, L. G.; Fokin, V. V.; Sharpless, K. B. *Angew. Chem., Int. Ed.* **2002**, *41*, 2596−2599.
(32) The effect of an aromatic solvent, like C_6D_6, on the spectral resolution in hyperbranched polymers was discussed earlier; see: Behera, G. C.; Ramakrishnan, S. *J. Polym. Sci., Part A: Polym. Chem.* **2007**, *45*, 1474−1480.
(33) Sunder, A.; Bauer, T.; Mülhaupt, R.; Frey, H. *Macromolecules* **2000**, *33*, 1330−1337.
(34) Dirand, M.; Bouroukba, M.; Briard, A. J.; Chevallier, V.; Petitjean, D.; Corriou, J. P. *J. Chem. Thermodyn.* **2002**, *34*, 1255−1277.
(35) Peleshanko, S.; Gunawidjaja, R.; Jeong, J.; Shevchenko, V. V.; Tsukruk, V. V. *Langmuir* **2004**, *20*, 9423−9427.
(36) Busse, K.; Peetla, C.; Kressler, J. *Langmuir* **2007**, *23*, 6975−6982.
(37) Sweet, Y. S.; Hedstrand, D. M.; Spinder, R.; Tomalia, D. A. *J. Mater. Chem.* **1997**, *7*, 1199−1205.
(38) Ornatska, M.; Bergman, K. N.; Rybak, B.; Peleshanko, S.; Tsukruk, V. V. *Angew. Chem., Int. Ed.* **2004**, *43*, 5246−5249.
(39) Miller, A.; Mohwald, H. *J. Chem. Phys.* **1987**, *86*, 4258−4265.
(40) Hossain, M. M.; Iimura, K.; Yoshida, M.; Kato, T. *J. Colloid Interface Sci.* **2011**, *353*, 220−224.
(41) Kasai, W.; Kuga, S.; Magoshi, J.; Kondo, T. *Langmuir* **2005**, *21*, 2323−2329.
(42) Hussain, S. A.; Chakraborty, S.; Bhattacharjee, D. *Indian J. Phys.* **2010**, *84*, 729−733.
(43) Schenning, A. P. H. J.; Roman, C. E.; Weener, J. W.; Baars, M. W. P. L.; Gaast, S. J. V.; Meijer, E. W. *J. Am. Chem. Soc.* **1998**, *120*, 8199−8208.
(44) Bangham, A. D. *Annu. Rev. Biochem.* **1972**, *41*, 753−776.
(45) Israelachvili, J. N.; Mitchell, D. J.; Ninham, B. W. *J. Chem. Soc., Faraday Trans. 2* **1976**, *72*, 1525−1568.